

RESEARCH

Open Access



A comparative investigation of the sorption of polycyclic aromatic hydrocarbons to various polydisperse micro- and nanoplastics using a novel third-phase partition method

Emeka Ephraim Emecheta^{1,2}, Diana Borda Borda¹, Patrizia Marie Pfohl³, Wendel Wohlleben³, Christoph Hutzler¹, Andrea Haase^{1*} and Alexander Roloff^{1*}

Abstract

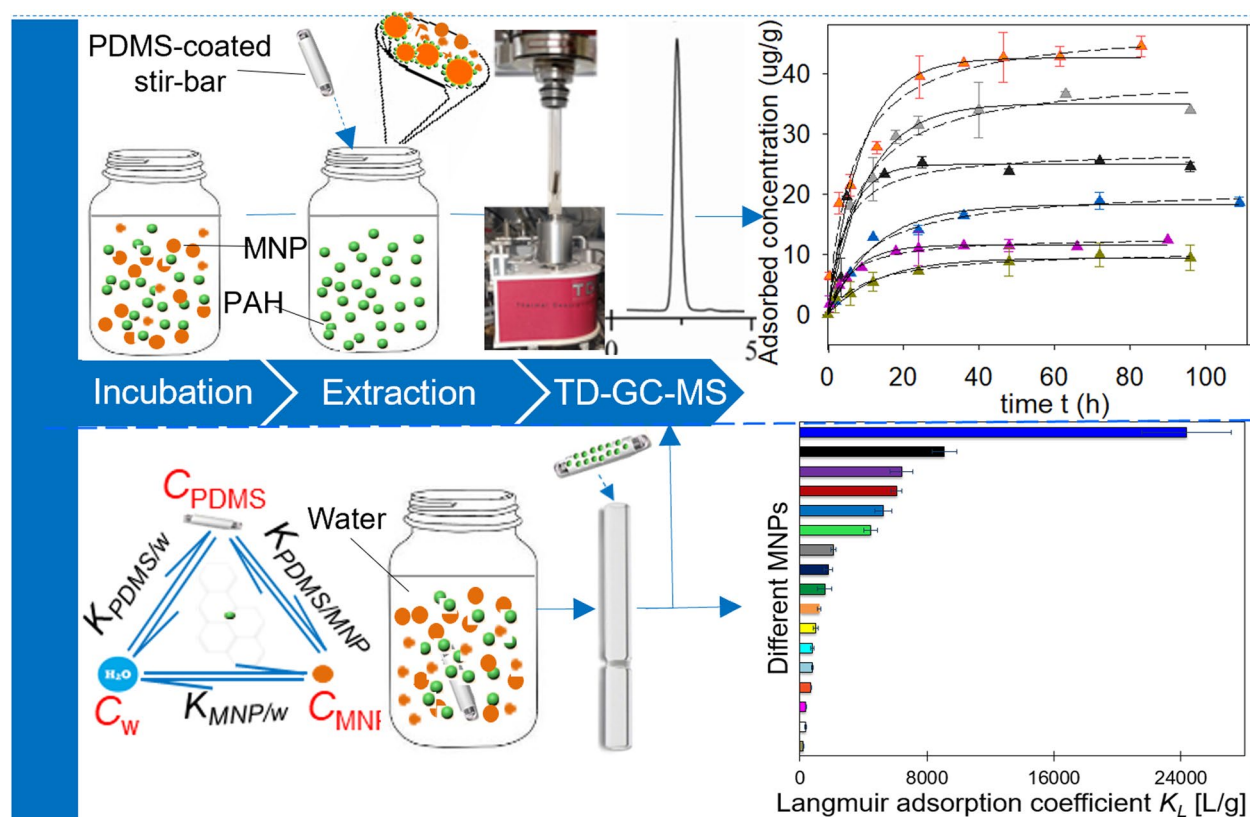
Evidence for direct adverse effects of micro- and nanoplastic particles (MNPs) on human health is scarce, but it has been hypothesized that MNPs act as carriers for environmental pollutants such as polycyclic aromatic hydrocarbons (PAHs). Many studies have already investigated the sorption of PAHs to microplastics, typically using the batch-equilibrium method. Here we established a novel third-phase partition (TPP) method utilizing thermo-extractable polydimethylsiloxane-coated stir-bars as re-usable passive samplers to compare the sorption of PAHs to 17 different MNPs. This method facilitates the quantification of MNP-sorbed pollutants, including those with poor water-solubility without requiring laborious filtration and solvent-extraction steps. Using benzo[*a*]pyrene (B[*a*]P) as a representative PAH, sorption kinetics and isotherms for MNPs were evaluated. B[*a*]P sorption was generally strong but differed by over two-orders of magnitude, clustering according to polymer types in the order of polyamides > polyethylenes >> Tire Rubber > polyurethanes > polymethyl methacrylate. B[*a*]P sorption was diminished for photo-aged MNPs. Within given polymer types, properties including particle size, polarity/hydrophobicity and chain mobility notably influenced B[*a*]P sorption. When comparing different PAHs, their sorption to selected MNPs increased over five-orders of magnitude with hydrophobicity: anthracene < B[*a*]P < dibenzo[*a,h*]pyrene. Our data is an important contribution to the understanding of the sorption behaviors of MNPs. The novel TPP-method represents a universally-applicable approach for the reliable evaluation of sorption characteristics of contaminants and MNPs, and can be easily adapted to desorption studies.

Keywords: sorption isotherms, sorption kinetics, microplastics, nanoplastics, PAHs, passive sampling, polymer aging

*Correspondence: andrea.haase@bfr.bund.de; alexander.roloff@bfr.bund.de

¹ German Federal Institute for Risk Assessment, Department of Chemical and Product Safety, Berlin, Germany
Full list of author information is available at the end of the article

Graphical Abstract



Introduction

Over the last decades, the demand for plastics has continued to rise with global production reaching 368 million tonnes in 2019 [1]. As a result of mainly mismanaged waste, plastic pollution has similarly grown and became a global health and environmental concern. Microplastics are either intentionally manufactured [2] or result from the fragmentation of bulk plastics into small-scale plastic debris [3–5]. Microplastics are ubiquitous [6]. They can be found in deep seas, soil, air and also in house dust [7–10]. Hence, ingestion and inhalation are plausible exposure routes to microplastics for humans [11–13]. Specific adverse effects have not yet been confirmed but uncertainties remain. For instance, the degradation of microplastics may yield even smaller nanoscaled particles that might differ with respect to uptake and biodistribution [14]. Clearly, the risk assessment of micro- and nanoplastic particles (MNPs) is hampered by analytical challenges and insufficient data [15]. In particular, the ability of MNPs to efficiently sorb hydrophobic toxic environmental pollutants may represent a potential hazard via a

transport that may or may not be significant compared to the transport via other vectors such as natural black carbon [16–19]. Environmental pollutants such as polycyclic aromatic hydrocarbons (PAHs) [20–22], heavy metals [23–26], polychlorinated biphenyls (PCBs) [27–29] and polybrominated diphenyl ethers (PBDEs) [30, 31] have been demonstrated to bind to microplastics. However, most studies used research-engineered polymer particles with a low degree of polydispersity, spherical shape and artificially high sorbate concentrations [20, 21, 32–35] that are unlikely to be found in the environment.

In contrast, we investigated MNPs with polydisperse and environmentally relevant size distributions. MNPs were obtained by cryomilling of polymer granules and separating the resulting particles applying different sieve sizes. In one specific case we also extracted particles from the fine fractions which are routinely removed from polymer powders being commercialized. These particles, though not present in the commercial products, feature realistic polymer compositions, polydispersities and non-spherical shapes and are representative of secondary

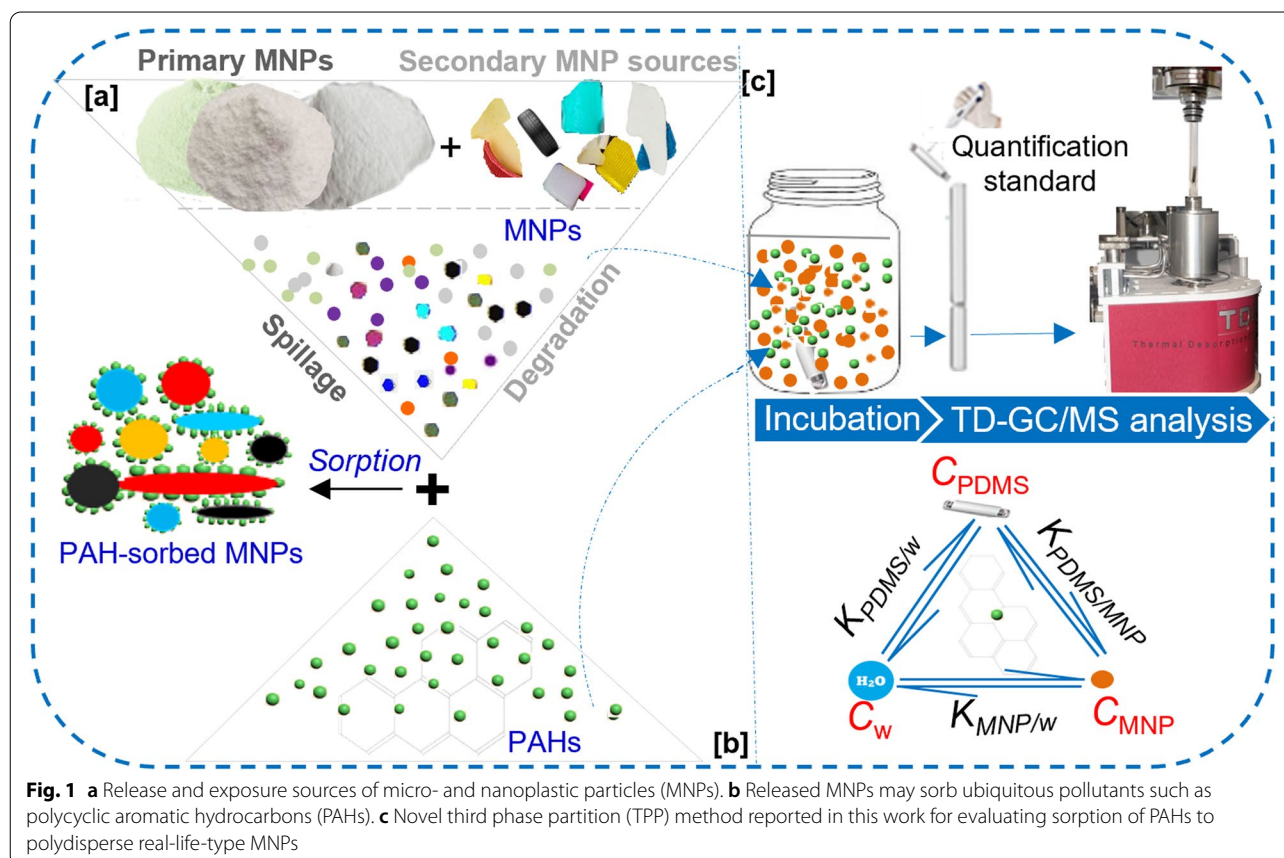
microplastics from environmental fragmentation, but lack aging. Therefore, selected MNPs were aged artificially using standardized methods and included in this investigation.

During their intended use in applications such as additive manufacturing (AM, better known as 3D-printing) [36–38], the polymer powders lose their particle shape by the selective local sintering with a laser (SLS process), but still, intermediate materials may enter the environment via spills during production, transport or disposal (Fig. 1a) and subsequently may sorb environmental pollutants (Fig. 1b). Understanding the sorption behaviors of these materials and persistent organic pollutants (POPs) may be helpful to establish grouping criteria for MNPs that could be useful in the context of plastics regulation [39], that is, if the fluxes of organic chemicals leaching from natural particles do not overwhelm the leaching from plastics, as it may be the case in many habitats [40].

Here we investigated the sorption kinetics and isotherms of MNPs being relevant for AM (polyamides – PAs, and thermoplastic polyurethanes – TPUs) and PAHs at environmentally relevant sorbate concentrations (ng/L). For comparison, recycled truck tire tread, polyurethanes (PUs) for outdoor applications as well as

polydisperse (low-density) polyethylene ((LD)PE) and polymethyl methacrylate (PMMA) were also evaluated (Table S1). Benzo[*a*]pyrene (B[*a*]P), a widespread environmental pollutant [41–43] and a mutagenic [44] and genotoxic [45] potential human carcinogen [46], was selected as a lead substance. In addition, anthracene (Anth) [47] and dibenzo[*a,l*]pyrene (DB[*a,l*]P) were included as structurally related PAHs with variable toxicities [47].

Sorption isotherms of particles are commonly investigated according to the batch-equilibrium method [30, 32, 35, 48]. This involves isothermal incubation of the target sorbent in a (typically aqueous) solution of the sorbate, followed by separation of the particles via filtration or centrifugation and quantification of the remaining solubilized sorbate fraction at equilibrium. Challenges arise from the incomplete removal of submicron-/nano-sized and/or low-density particles through filtration or centrifugation. Furthermore, hydrophobic sorbates with low water-solubilities might result in equilibrium concentrations too small to be accurately measured. Moreover, the batch-equilibrium method is time-consuming, labor-intensive and requires large amounts of organic solvent for sample extraction.



To bypass these challenges, we developed a novel and sensitive third-phase partition (TPP) method for evaluating the sorption of PAHs to polydisperse real-life-type MNPs (Fig. 1c). The TPP method covers PAH concentrations in the ng/L-range that can be adequately measured [49–51] with minimal sample preparation and without the consumption of significant amounts of organic solvents. Thus, error-prone filtration, centrifugation and extraction steps are omitted, increasing the reliability of results. Inspired by previous work on passive sampling [52], the method relies on partitioning of PAHs in a three-phase system comprised of water, MNPs and a re-usable polydimethylsiloxane (PDMS) coated stir-bar. Quantification of the PAHs partitioned to the PDMS phase is achieved via automated online-coupled thermal desorption gas chromatography mass spectrometry (TD-GC-MS), from which sorption isotherms can be derived (see method section and the supplementary information (SI) for details). Compared to the batch-equilibrium method and to previously reported TPP approaches [20, 28, 52, 53], the need for laborious solvent extraction is eliminated and the analysis time is significantly reduced. Importantly, this approach also allows to study very hydrophobic pollutants featuring strong binding to MNPs, such as DB[*a,l*]P, if their PDMS/water partition coefficients ($K_{PDMS,w}$) are known. To the best of our knowledge, this is the first study utilizing a passive sampling approach combined with automated online-coupled TD-GC-MS to evaluate the sorption kinetics and isotherms of microplastics that also contain submicron fractions.

Materials and methods

Chemicals

B[*a*]P (purity $\geq 99.5\%$) was purchased as a standard solution in cyclohexane from Sigma-Aldrich (Steinheim, Germany). Benzo[*a*]pyrene-*d*₁₂ (B[*a*]P-*d*₁₂), Anth, anthracene-*d*₁₀ (Anth-*d*₁₀), DB[*a,l*]P and dibenzo[*a,i*]pyrene (DB[*a,i*]P) were purchased as analytical standards in acetonitrile (purity $\geq 98.5\%$) from Neochema (Bodenheim, Germany). Acetonitrile, hexane, methanol and dichloromethane in analytical grade were purchased from Merck (Darmstadt, Germany) and used as solvents. Nitrogen and helium of $\geq 99.999\%$ purity were purchased from Linde (Pullach, Germany). Ultrapure water from a Millipore Q-POD® dispenser connected to a Millipore milli-Q system (Darmstadt, Germany) was used.

Materials and devices

250 mL amber glass vials (Duran group, Mainz, Germany) were utilized for all experiments. Transparent 250 mL vials were wrapped with aluminum foil where amber vials were unavailable. All vials were sealed

air-tight during experiments with polytetrafluoroethylene (PTFE) coated screw caps (Duran group, Mainz, Germany). Cimarec multipoint stirring plates (ThermoFisher Scientific, Germany) operating at 600 rotations per minute (rpm) were used for all incubations inside a light-protected and temperature-controlled chamber (Binder GmbH, Tuttlingen, Germany) which was operated at 21°C. Temperature stability inside the incubation chamber was characterized by continuous temperature monitoring using a temperature sensor which was placed inside the 250 mL glass vial and connected to an automated data logger system (ELPRO, Schorndorf, Germany). All filtrations were performed with 1.2 µm GF/C Whatman glass microfiber filters. PDMS-coated magnetic stir-bars (Twister®) with a PDMS film thickness of 0.5 mm, lengths of 10 and 20 mm, PDMS phase volumes of 24 and 126 µL and densities of 965 kg/m³ were purchased from Gerstel (Mühlheim, Germany) and used as passive samplers. Thermal desorption (TD) glass tubes (length: 60 mm), transport adapters as well as the thermal conditioner 2 (TC 2) connected to an AUX 163 controller were all from Gerstel. Kimtech Science white precision wipes (Kimberly-Clark Professional, Germany) and Solingen tweezers (Kiehl Solingen, Germany) were used for handling the PDMS-coated stir-bars in order to avoid contamination. Details about quality control, cleaning and conditioning procedures for the PDMS-coated stir-bars and glassware are detailed in Section S1 in the SI.

Micro- and nanoplastic particles investigated in this study

Sorption kinetics and isotherms for PAHs and MNPs were investigated for 17 different particle types. Names and median size distributions of MNPs are listed in Table 1. (LD)PE particles were obtained from LyondellBasell (Frankfurt, Germany) and Cospheric (Santa Barbara, USA). PMMA particles were purchased from Polysciences (Warrington, USA), and micronized Tire Rubber was obtained from MRH (Mülsener Rohstoff- und Handelsgesellschaft mbH, Mülsen, Germany). Non-crosslinked TPU (elastomer), crosslinked PU (durometer) and PA particles were supplied by BASF SE (Ludwigshafen am Rhein, Germany). The MNPs were obtained by cryo-milling of polymer granules and sieving the resulting material with different sieve sizes to obtain smaller particle fractions. The particles are generally polydisperse; therefore, additional sieving was introduced to produce a cut-off for the particles within a given distribution. Details about the particles and their physiochemical properties are presented in Table S1. Melting temperatures (T_m) and glass transition temperatures (T_g) were obtained using differential scanning calorimetry (DSC) on a Q2000 instrument (TA Instruments, Eschborn, Germany). Samples were heated from -50 to 300°C

Table 1 MNPs investigated in this study and corresponding average size distributions. Detailed physical-chemical properties of all MNPs are summarized in Table S1

Name	Dx10 (μm)	Dx50 (μm)	Dx90 (μm)
LDPE_215	96.2	215.0	380.
LDPE_84	19.1	84.0	188.0
PE_0.6	0.3	0.6	1.9
TPU_ester_arom	142.0	254.0	418.0
TPU_ester_alip	143.0	262.0	440.0
TPU_ether_arom	128.0	246.0	413.0
TPU_ether_alip	152.0	267.0	442.0
TPU_melt_arom	272.0	864.0	1560.0
PU_foam	33.1	92.8	211.0
PU_arom_1C	82.8	200.0	354.0
PU_arom_2C	77.2	201.0	368.0
PA-6_7	2.3	6.9	13.5
PA-6_42	13.7	42.2	75.3
PA-12_44	34.4	44.3	57.0
PMMA_0.3	0.3	0.3	0.4
PMMA_6	2.2	6.2	11.6
Tire Rubber	61.7	130.0	233.0

Dx10, Dx50 and Dx90 are the 10th, 50th and 90th percentile average size distributions, respectively

at 10°C/min. Brunauer-Emmett-Teller (BET) surface areas of the particles were analyzed with a micromeritics instrument (Norcross, USA). Nitrogen adsorption isotherms were obtained at a temperature of 77 K, an equilibrium time of 5 s and a saturation pressure of 770 mmHg. Sample masses of 0.17–2.5 g were used. Particle size distributions of MNPs were measured via laser diffraction utilizing a Malvern Mastersizer 3000 (Kassel, Germany). Particles were measured in 10 replicates in dispersions containing water plus two drops of Nekanil 910 as a surfactant to stabilize the dispersions (BASF SE, Ludwigshafen, Germany). The average size distributions of the particles are presented as 10th (D×10), 50th (D×50) and 90th (D×90) percentiles.

To evaluate the effect of MNP aging on PAH sorption, three selected MNPs (LDPE_215, PA-6_42 and Tire Rubber) were artificially aged via exposure to ultraviolet (UV) light. About 0.5–0.7 g of the sample were placed inside a petri dish to form a monolayer powder. The samples were aged without mixing for 1000 and 2000 h inside a Suntest XLS+ chamber (Atlas, Illinois, USA) according to the DIN EN ISO 4892 guideline (sunlight spectrum, UV intensity of 60 W/m² in the wavelength range of 300–400 nm, Black Standard Temperature of 65°C, no rain events) [54]. Fourier transform infrared (FTIR) spectroscopy was carried out on a ThermoFisher IS50 FT-IR spectrometer equipped with a diamond attenuated total reflectance (ATR) accessory (IS50-ATR) and was utilized to evaluate the aged MNPs and their non-aged versions for changes

in their functional groups. As described in earlier studies [55], the FT-IR spectra were recorded in the region of 4000–400 cm⁻¹ with 32 scans at a resolution of 4 cm⁻¹.

Quantification of polycyclic aromatic hydrocarbons via online-coupled thermal desorption gas chromatography mass spectrometry (TD-GC-MS)

TD-GC-MS is a three-stage process involving TD of substances loaded onto the PDMS-coated stir-bar, followed by separation of the desorbed substances via GC and MS detection. TD was performed with a thermal desorption unit (TDU 2, Gerstel) connected to a 6890 series gas chromatograph that was coupled with a 5975 series mass selective detector (both Agilent, Waldbronn, Germany). The TDU was operated with a helium gas flow of 290 mL/min and a temperature program starting at 60°C for 0.1 min, then increasing to 290°C at 40°C/min and then holding that temperature for 5 min. During TD, which was performed in split mode with a split ratio of 35:1 in the TDU, analytes were cryo-focused with liquid nitrogen at -100°C in the cold injection system (CIS 4; Gerstel). The CIS, which was directly connected to the TDU, was equipped with a liner packed with deactivated glass wool (Gerstel). The CIS was operated in split mode of 35:1 ratio (combined split of 1:1225 from TDU and CIS), a split flow of 35 mL/min and an inlet pressure of 149 kPa. After desorption and cryo-focusing, the CIS inlet was rapidly heated to 320°C at 12°C/s and then held for 5 min. The TDU to CIS transfer temperature was 350°C.

The GC was equipped with a DB-EUPAH column of 20 m length, an inner diameter of 0.18 mm and film thickness of 0.14 μm (J & W Scientific, Folsom, U.S.). Helium gas was used as a carrier gas at a constant flow of 1.0 mL/min. The GC oven was operated with a temperature program starting at 60°C for 0.5 min, followed by heating to 180°C at 15°C/min and finally to 320°C at 12°C/min, where the temperature was held for 8 min.

The temperatures of the quadrupole, ion source, and MS transfer line were 150, 230 and 320°C, respectively. The MS detector was operated in combined selective ion monitoring (SIM) and scan mode with a scan rate of 15.99/s. A range of 50–500 m/z was monitored for data acquisition. During SIM data acquisition, two ions were monitored for each analyte: 178 and 176 m/z for Anth, 188 and 187 m/z for Anth- d_{10} , 252 and 250 m/z for B[a]P, 264 and 260 for B[a]P- d_{12} and 302 and 300 m/z for DB[a,l]P and DB[a,i]P as quantifier and qualifier ions, respectively. Each ion was monitored with a dwell time of 10 milliseconds.

Quantification of target PAHs were achieved via calibration. A known amount of PAHs and 100 ng of the correlated internal standards (Anth- d_{10} for Anth, B[a]P- d_{12} for B[a]P and DB[a,i]P for DB[a,l]P) were spiked on the surface of pre-cleaned PDMS-coated stir-bars. The stir-bars were held with tweezers until the solvent was fully evaporated and then introduced into TD glass tubes and capped with a transport adapter. The calibrations were linear for concentration ranges of 2.5–500 ng for Anth and B[a]P and 5–250 ng for DB[a,l]P. Exemplary calibration curves are shown in Figure S1. In between every sample and calibration run, the system was purged by performing a blank run (Section S1).

Determination of kinetic and sorption isotherms of PAHs and MNPs in water via a third-phase partition method

Before measuring sorption isotherms of the MNPs, kinetics experiments were firstly conducted to establish the time required for the PAHs to partition to the PDMS (Section S2). Secondly, to establish the time required for the PAHs to reach equilibrium with the MNPs in water, kinetics experiments were performed as described in Section S2 with slight modifications. 5 mg of target MNPs were incubated in 240 mL water spiked with 1 $\mu\text{g/L}$ target PAH in replicate vials. A regular magnetic stir-bar (without PDMS coating) was utilized to stir the dispersions at 600 rpm inside the incubation chamber at 21°C. At specified time intervals up to 132 h, duplicate vials were withdrawn from the stirring plate and the sample mixture was filtered to separate the MNPs from the aqueous phase. The filtrate was analyzed via stir-bar sorptive extraction (SBSE). To account for losses due to filtration and possible

photo-degradation of PAHs, control samples containing 1 $\mu\text{g/L}$ of the target PAH but no MNPs were incubated under identical conditions. For each time point, recovery-corrected concentrations of the control samples were used as initial concentration, C_0 ($\mu\text{g/L}$). After incubation, the PDMS-coated stir-bars were analyzed via TD-GC-MS. The concentration of PAH sorbed to the MNPs at each time point, $C_{MNP,t}$ ($\mu\text{g/kg}$), was calculated as follows:

$$C_{MNP,t} = \frac{C_0 - C_{w,t}}{M_{MNP}} V_w, \quad (1)$$

where $C_{w,t}$ ($\mu\text{g/L}$), V_w (L) and M_{MNP} (kg) are the aqueous PAH concentration at time point t , the volume of water and the mass of MNPs, respectively.

Sorption isotherms characterizing the sorption behavior of PAHs and MNPs were obtained using the TPP method (see Fig. 1c). PAHs will distribute between water, MNPs and the PDMS coating on the stir-bar according to their respective partition coefficients K (L/kg). These are defined as the PAH concentration ratios between two phases at chemical equilibrium, e.g.

$$K_{MNP/w} = \frac{C_{MNP}}{C_w}. \quad (2)$$

The PAH concentration in the aqueous phase, C_w ($\mu\text{g/L}$), was derived from

$$C_w = \frac{C_{PDMS}}{K_{PDMS/w}}, \quad (3)$$

where C_{PDMS} ($\mu\text{g/kg}$) is the measured concentrations of PAHs in the PDMS phase, and $K_{PDMS/w}$ (L/kg) are the partition coefficients of PAHs for PDMS and water, which was determined experimentally (Anth, B[a]P) or calculated (DB[a,l]P, see Section S2 for details).

The PAH concentration in the MNP phase, C_{MNP} ($\mu\text{g/kg}$), was calculated from the total amount of PAH in the system m_{total} (μg), C_w , C_{PDMS} and other characteristic parameters of the system assuming mass balance according to

$$C_{MNP} = \frac{1}{M_{MNP}} \left(m_{total} - \frac{C_{PDMS}}{K_{PDMS/w}} V_w - C_{PDMS} M_{PDMS} \right), \quad (4)$$

where M_{PDMS} (kg), M_{MNP} (kg) and V_w (L) are the mass of the PDMS phase, the mass of MNPs and the volume of water in the system, respectively.

All isotherms were derived from 5–7 different PAH equilibrium concentrations in duplicate or triplicate to obtain between 10–21 data points per individual isotherm. Sorption experiments were performed in 240 mL water using stir-bars with 24 μL PDMS-phase volume. Details are summarized in Table S2. In brief, aqueous mixtures

containing MNPs, PAHs of various initial concentrations and a PDMS-coated stir-bar were incubated by continuous stirring until chemical equilibrium of all components of the system was approached. Organic solvents from PAH stock solutions were kept $\leq 0.03\%$ (v/v), which has previously been demonstrated to yield negligible co-solvent effects [52, 56, 57]. The stir-bar was removed from the vial with clean tweezers, briefly washed with distilled water and gently wiped with a lint-free tissue to remove water and polymer residues. Subsequently, the stir-bar was spiked with 100 ng of the appropriate internal standards, held with tweezers until the solvent was fully evaporated, inserted into TD glass tubes and finally analyzed via TD-GC-MS for C_{PDMS} .

Quality control measures undertaken to mitigate the loss of the PAH sorbate during incubation and control experiments to verify the conservation of PAH mass are outlined in Sections S1 and S2, respectively. The combined measurement uncertainties of $K_{MNP/w}$ determined via the TPP-method were calculated according to the international standard organization (ISO) Guide to the Expression of Uncertainty in Measurement (GUM) [58]. Additionally, the contribution of each component used to calculate of $K_{MNP/w}$ to the combined uncertainties was calculated (see Section S6 for details).

Data analysis

TD-GC-MS data were acquired and processed with MassHunter software (Agilent, versions B.06.00 and B.05.00). Microsoft Excel 2016 was used for additional data processing. Model fittings were performed by non-linear regression methods using SigmaPlot 14 software application (Systat Software Inc, USA) while two-tailed t-test analysis of the data was performed with GraphPad Prism 9 (GraphPad Software, USA).

Experimentally derived kinetics for the sorption of PAHs to MNPs (Section S3) were fitted by applying pseudo-first (Eq. 5) and pseudo-second (Eq. 6) order models, respectively [21, 32]:

$$C_w = \frac{C_{PDMS}}{K_{PDMS/w}}, \quad (5)$$

$$C_w = \frac{C_{PDMS}}{K_{PDMS/w}}, \quad (6)$$

where k_a (h^{-1}) and k_b ($\text{g } \mu\text{g}^{-1} \text{ h}^{-1}$) are rate constants from both models while q_e is the calculated equilibrium sorption capacity.

The goodness of the model fittings was evaluated using the coefficient of determination (R^2) and Chi-square (χ^2)

parameters. Better fittings result in R^2 values approaching unity and smaller values for χ^2 (Section S3, Table S3).

Experimental sorption isotherm data were fitted to eight different isotherm models and compared for their goodness of fit and plausibility of parameters. Exemplary isotherm fittings and corresponding model-parameters for PAH sorption to PA-6_42 are shown in Figure S4. The Langmuir model (Eq. 7) was found most suitable to compare the sorption of the PAHs to MNPs across the tested concentration ranges, and can be utilized to compare different sorbents by means of their Langmuir adsorption coefficients K_L (L/kg) and theoretical maximum monolayer adsorption capacities q_{max} ($\mu\text{g/kg}$) [59], where $K_L = \alpha_L \cdot q_{max}$ (α_L (L/ μg) is the Langmuir isotherm constant).

$$C_{MNP} = \frac{K_L \cdot C_w}{1 + \alpha_L \cdot C_w}. \quad (7)$$

We note that the Langmuir model assumes that PAHs bind to MNPs via monolayer surface adsorption, which will most likely not be the case for each of the investigated polymers. Rubbery polymers, in particular, will probably take up PAHs by true partitioning in addition to surface adsorption. Still, the Langmuir model allows to extract comparable (and concentration-independent) physico-chemical parameters for a wide range of MNPs and PAHs, which justified its use in this study.

Results and discussion

The polymer type mainly determines sorption of benzo[a]pyrene to micro- and nanoplastic particles

Initially, the kinetics and isotherms for partitioning of PAHs between water and PDMS in the passive samplers were determined (Figure S2, see Section S2 for details). The slopes of the linear isotherms represent the partition coefficients $K_{PDMS/w}$, which are required to calculate PAH concentrations on MNPs (C_{MNP}) from measured concentrations in PDMS (C_{PDMS}) according to Eq. 4. Values for $\log K_{PDMS/w}$ were increasing from 4.05 ± 0.09 for Anth to 5.10 ± 0.10 for B[a]P. This is in line with values reported previously for the same polymer [60]. Due to the very low water solubility of DB[a,l]P, $\log K_{PDMS/w}$ for this PAH was calculated to be 6.88 according to Equation S2 [61], which correlates $\log K_{PDMS/w}$ with the logarithmic octanol/water partition coefficient $\log K_{o/w}$. Notably, the same correlation yielded a value for $\log K_{PDMS/w}$ of 5.0 for B[a]P. This is in good agreement with the experiment, supporting the validity of Equation S2 for substances with $\log K_{o/w} > 4$.

Kinetics experiments to study PAH sorption to selected MNPs were conducted according to the batch-equilibrium method, revealing equilibration times of 48 h for the sorption of B[a]P, Anth and DB[a,l]P under the conditions applied (Fig. 2 and Section S3). Two of the most common kinetics models for sorption processes,

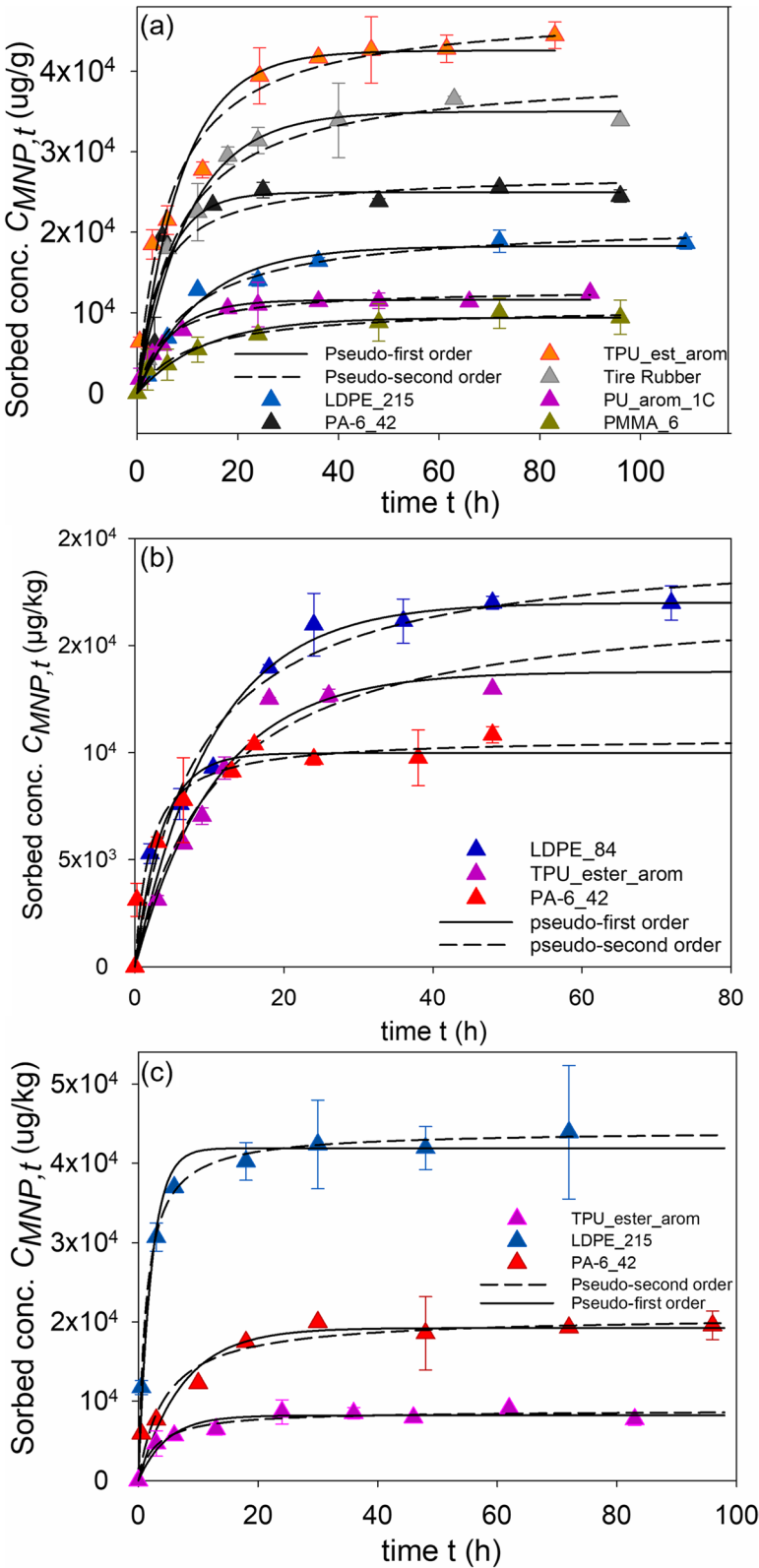
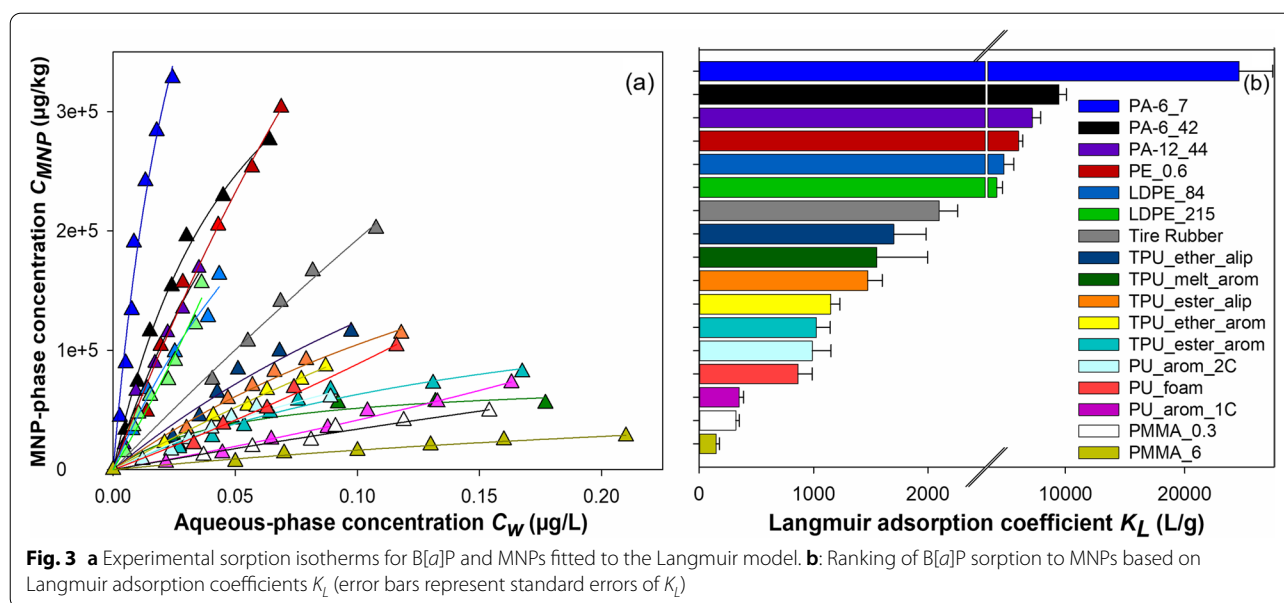


Fig. 2 Sorption kinetics of (a) B[a]P, (b) Anth and (c) DB[a,l]P and selected MNPs ($n = 2 \pm \text{SD}$) fitted to pseudo-first and pseudo-second order kinetics models. See Table S3 for model parameters and calculated rate constants



the pseudo-first and pseudo-second-order models [62, 63], were both suitable to describe the observed sorption kinetics processes, with no significant difference ($p < 0.01$) between them (see also Figure S3 and Table S3). This further suggests that diffusion-driven mass transfer of the sorbate to the sorbent or sorption onto the active sites of the sorbent or both phenomena may be the rate-limiting steps of the sorption process [32, 64].

We went on to compare the sorption isotherms of various MNPs utilizing B[a]P as a representative PAH sorbate. Sorption isotherms were obtained by means of the novel TPP method. Accordingly, MNPs were incubated together with a PDMS-coated stir-bar in aqueous solutions of varying initial B[a]P concentrations until equilibrium of the system was approached. C_{PDMS} was then determined via TD-GC-MS, which revealed C_{MNP} (Eq. 4) and C_w (Eq. 3). Plots of C_{MNP} as a function of C_w representing sorption isotherms were then fitted to the Langmuir model (Fig. 3a, see Section S4 for details). For Anth, B[a]P and selected MNPs, the sorption isotherms and corresponding Langmuir adsorption coefficients K_L acquired with the TPP-method were validated using the batch-equilibrium method (Section S5). This confirmed the TPP-method presented herein as an easy, fast and reliable alternative for evaluating the sorption properties of organic pollutants and MNPs.

As illustrated in Table 2, K_L differed by more than two orders of magnitude for B[a]P, ranging from 150 L/g for PMMA_6 to 25000 L/g for PA-6_7. In addition, the values of the Langmuir separation factor R_L were < 1 , suggesting a favorable and reversible

sorption process for all investigated MNPs [65]. As shown in Fig. 3b, K_L values for the different MNPs cluster according to the ‘polymer type’, decreasing in the order of PA-6 > PA-12 > (LD)PE \gg Tire Rubber > (T)PUs > PMMA. This ranking suggests that the polymer type which governs the essential chemical and some physical characteristics of the MNPs is a key factor influencing the sorption of B[a]P. For example, the exceptionally high sorption of B[a]P by PA-6 MNPs is possibly related to the high water absorption capacity of this polymer (up to 9.5%) [66], which is significantly higher than for some of the other investigated materials (0.2–1.5% for PA-12, PE, and TPUs) [66, 67]. This could facilitate the transport of dissolved B[a]P to the bulk of the material.

In contrast, PA-12 MNPs yielded strong sorption of B[a]P despite this polymer’s notably lower water absorption capacity [67]. However, PA-12 MNPs featured a relatively high specific surface area ($0.73 \text{ m}^2/\text{g}$, see Table S1), which may favor surface-pore adsorption typical for glassy polymers [68, 69]. Additionally, PA-12 is characterized by a reduced polarity due to longer alkyl chains and lower surface amide densities, which is reflected in higher water contact angles compared to PA-6 [67]. This may render the displacement of water molecules from potential sorption sites on this polymers’ surface by B[a]P energetically more favorable.

Similarly, strong B[a]P sorption was observed for (LD) PE particles. (LD)PE is a rubbery polymer with a glass transition temperature T_g well below room temperature (Table S1) and consists of flexible amorphous regions [70], which facilitate the mobility of sorbates within the

Table 2 Langmuir model parameters of isotherms characterizing the sorption of PAHs to MNPs

Sorbate	Sorbent	Langmuir model Parameters					Error functions	
		$K_L \pm S.E$ (L/kg)	$\log K_L \pm S.E$	α_L (L/ μ g)	q_{max} (μ g/g)	R_L	R^2	χ^2 [μ g/g]
DB[a,]P	PA-6_42	$1.0E+09 \pm 8.5E+07$	9.0 ± 0.1	5370.92	192	0.0001	0.991	1.6
	LDPE_215	$2.3E+08 \pm 2.5E+07$	8.4 ± 0.1	1123.67	207	0.0004	0.988	5.3
	TPU_ester_ arom	$7.0E+07 \pm 1.1E+07$	7.8 ± 0.1	706.91	99	0.0007	0.973	2.1
Anth	PA-6_42	$1.1E+05 \pm 9.3E+03$	5.0 ± 0.1	0.10	1136	0.003	0.989	4.5
	LDPE_215	$3.1E+04 \pm 2.7E+03$	4.5 ± 0.1	0.15	205	0.011	0.992	5.8
	TPU_ester_ arom	$8.7E+03 \pm 2.0E+03$	3.9 ± 0.2	0.01	694	0.026	0.963	2.0
B[a]P	PA-6_7	$2.5E+07 \pm 2.8E+06$	7.4 ± 0.1	31.0	788	0.009	0.981	15.7
	PA-6_42	$9.5E+06 \pm 7.9E+05$	7.0 ± 0.1	16.84	562	0.016	0.990	14.3
	PA-6_42_1000h	$9.5E+06 \pm 1.1E+06$	7.0 ± 0.1	16.81	565	0.01	0.990	4.3
	PA-6_42_2000h	$8.0E+06 \pm 2.4E+06$	6.9 ± 0.3	16.44	489	0.01	0.927	28.9
	PA-12_44	$7.2E+06 \pm 7.1E+05$	6.9 ± 0.1	17.66	408	0.015	0.989	7.1
	PE_0.6	$6.1E+06 \pm 3.4E+05$	6.8 ± 0.1	5.81	1045	0.033	0.998	0.8
	LDPE_84	$4.8E+06 \pm 5.2E+05$	6.7 ± 0.1	8.66	560	0.030	0.993	1.0
	LDPE_215	$4.2E+06 \pm 4.5E+05$	6.6 ± 0.1	6.16	689	0.051	0.980	5.0
	LDPE_215_1000h	$1.5E+06 \pm 1.3E+05$	6.2 ± 0.1	3.82	391	0.06	0.996	2.1
	LDPE_215_2000h	$1.9E+06 \pm 5.6E+05$	6.3 ± 0.3	3.04	624	0.08	0.961	60.5
	Tire Rubber	$2.1E+06 \pm 1.6E+05$	6.3 ± 0.1	0.88	2380	0.232	0.995	1.2
	Tire Rubber_1000h	$1.3E+06 \pm 4.8E+04$	6.1 ± 0.03	4.02	330	0.06	0.999	0.2
	Tire Rubber_2000h	$9.9E+05 \pm 1.5E+05$	6.0 ± 0.1	1.68	590	0.13	0.984	136.9
	TPU_ether_alip	$1.7E+06 \pm 2.8E+05$	6.2 ± 0.1	3.72	457	0.082	0.968	8.6
	TPU_melt_ arom	$1.6E+06 \pm 3.7E+05$	6.2 ± 0.2	20.11	77	0.016	0.980	3.5
	TPU_ester_alip	$1.5E+06 \pm 1.0E+05$	6.2 ± 0.1	4.05	364	0.076	0.992	0.9
	TPU_ether_ arom	$1.1E+06 \pm 1.1E+05$	6.1 ± 0.1	1.89	608	0.150	0.996	0.5
	TPU_ester_ arom	$1.0E+06 \pm 4.5E+04$	6.0 ± 0.04	6.16	166	0.039	0.972	4.5
	PU_ arom_2C	$9.9E+05 \pm 1.7E+05$	6.0 ± 0.1	4.32	229	0.072	0.953	4.1
	PU_foam	$8.6E+05 \pm 7.0E+04$	5.9 ± 0.1	1.07	808	0.238	0.971	11.0
	PU_ arom_1C	$3.5E+05 \pm 3.4E+04$	5.5 ± 0.1	-1.38	-255	-0.320	0.984	2.5
	PMMA_0.3.	$3.2E+05 \pm 5.1E+04$	5.5 ± 0.1	-1.33	-241	-0.250	0.989	1.0
	PMMA_6	$1.5E+05 \pm 2.4E+04$	5.2 ± 0.1	-1.62	-91	-0.259	0.951	3.2

K_L , S.E, q_{max} , a_L and R_L are the Langmuir adsorption coefficient, the standard error of K_L , the theoretical maximum adsorption capacity, the Langmuir adsorption constant and the dimensionless separation factor, respectively. R^2 and χ^2 are the coefficient of determination and Chi-square errors, respectively

polymer network. Therefore, it is likely that the observed strong sorption is due to the migration of B[a]P into the bulk of the polymer (true partitioning) in addition to surface adsorption [71–73]. On the other hand, PMMA and PU_ arom_1C, being glassy polymers at room temperature ($T_{g(PMMA)} = 41^\circ\text{C}$, $T_{g(PU_ arom_2C)} = 31^\circ\text{C}$, Table S1), exhibited the lowest sorption of B[a]P of all polymers, possibly due to their rigid and condensed structure [74, 75] resulting in slow diffusion that is typical for glassy

polymers [76]. Further investigations may reveal the extent to which each individual property affects sorption, and to which extent adsorption to the surface and absorption to the bulk play a role for individual polymer types.

In general, K_L values for all investigated MNPs are well above 10^5 L/kg, which points to efficient sorption of B[a]P to the investigated polymer particles in aqueous systems.

Additional factors influencing sorption of benzo[a]pyrene to micro- and nanoplastic particles

For selected polymer types, the effects of different physico-chemical properties on B[a]P sorption to MNPs were investigated.

Initially, the effect of particle size and surface area was evaluated for PMMA, (LD)PE, and PA-6. As expected, a significant increase in K_L was observed with decreasing mean particle size (Fig. 4a) for all studied sub-sets. The smaller PA-6_7 MNPs were characterized by a 2.7-fold higher K_L compared to the larger PA-6_42 variants. Regarding (LD)PE, a steady increase in K_L was observed with decreasing particle size. Similarly, K_L for PMMA_0.3 was over 2-fold higher compared to PMMA_6. However, the measured BET surface area for the same MNPs decreased by 10-fold from 15.0 to 1.6 m²/g, suggesting a limited dependence of sorption on the surface area. The plot in Fig. 4b indicates that the dependency of the Langmuir adsorption coefficients of B[a]P on the measured BET surface area is particularly relevant within a given polymer type, but not so much between them. The size distribution of the MNPs usually determines the specific surface area and, thus, the number of available adsorption sites on the particle surface [77]. Consequently, smaller particles usually display increased surface adsorption capacities [21, 78]. However, the strength of individual binding interactions will be governed by chemical properties reflected by the polymer type, which could explain the observed differences. In addition, it should be emphasized that the partitioning into the bulk will likely play a significant role for many of the studied MNPs, which will be reflected in a dependency on particle volume rather than surface area. However, since MNPs in this work are polydisperse, a reliable determination of average particle volumes is challenging.

Among the investigated TPUs, log K_L ranged from 6.01 to 6.23 (Table 2). These materials have very similar physico-chemical properties, including similar glass transition temperatures T_g below room temperature. Such polymers are typically classified as rubbery polymers and are characterized by a larger free volume and a higher flexibility and mobility of their molecular chains [73, 79]. However, the TPUs differ in their chain segments, which were polymerized from aromatic or aliphatic isocyanates in the 'hard' segment and included polyester or polyether chains in the 'soft' segment. TPUs with aliphatic (rather flexible) hard-segments were characterized with significantly higher K_L values compared to their aromatic (rather rigid) counterparts, potentially as a result of the better accessibility for PAHs to the polymer bulk provided by the more flexible polymer chains (Fig. 4c). We also observed that polyether-based TPUs sorbed slightly higher concentrations of B[a]P than polyester-based

TPUs, irrespective of the composition of their hard segments. Aliphatic residues and ether moieties are supposed to reduce the polarity of TPU MNPs, thereby favoring the displacement of water molecules from their hydration shells with B[a]P. In addition, the influence of the soft and hard segments of TPU polymers were compared. TPU_melt_ arom is mainly composed of the polyester soft segment and contains only a minute fraction of the rather rigid aromatic hard segment, while TPU_ ester_ arom contains almost equal proportions of hard and soft segments. B[a]P sorption by TPU_melt_ arom was slightly higher (ca. 1.5-fold) compared to TPU_ ester_ arom (Fig. 4c). This is despite the larger median particle size of the former (Table S1). Notably, TPU_melt_ arom has a low T_m of 52°C as well as a low T_g of -49°C. This implies amorphous behavior and high mobility of the molecular chains which could favor partitioning of B[a]P to the polymer bulk. Overall, the aforementioned effects are indicative of sorption significantly influenced by bulk partitioning of B[a]P.

Photo-aging of micro- and nanoplastics reduces sorption of benzo[a]pyrene

Prolonged exposure of MNPs to environmental weathering conditions may cause changes in their (surface) properties during the lifecycle, which can alter the sorption behavior of organic pollutants. In this work, we investigated how accelerated photo-aging of selected MNPs affects the sorption of B[a]P. MNPs were exposed to prolonged UV light irradiation (60 W/m², 300–400 nm) for 1000–2000 h which is supposed to simulate roughly one year of exposure to sunlight in Europe. Photo-aging significantly reduced B[a]P sorption to LDPE_215 and Tire Rubber (Fig. 5a /b). For example, K_L of LDPE_215 MNPs decreased 3.2-fold after 1000 h of UV light exposure, which did not further change after 2000 h. Similarly, B[a]P sorption to Tire Rubber particles decreased by over 2.1-fold after 2000 h. No significant difference was observed for sorption of B[a]P to PA-6 after photo-aging, despite the notable effect that photo-aging had on the IR spectrum of these particles (Fig. 5c). We hypothesize that photo-aging of PA-6 MNPs did not significantly affect the water absorption capacity of these polymer particles and, therefore, transport of dissolved B[a]P into the bulk remains similar.

The decreased K_L values for aged LDPE_215 and Tire Rubber might reflect alterations in surface functional groups, most likely caused by reactions with oxygen following photo-excitation. The incorporation of hydroxyl, carbonyl or carboxyl groups render the surface of the aged MNPs more hydrophilic. This was confirmed by FTIR-spectroscopy, were typical bands for oxygen-containing functional groups were observed at wavenumbers

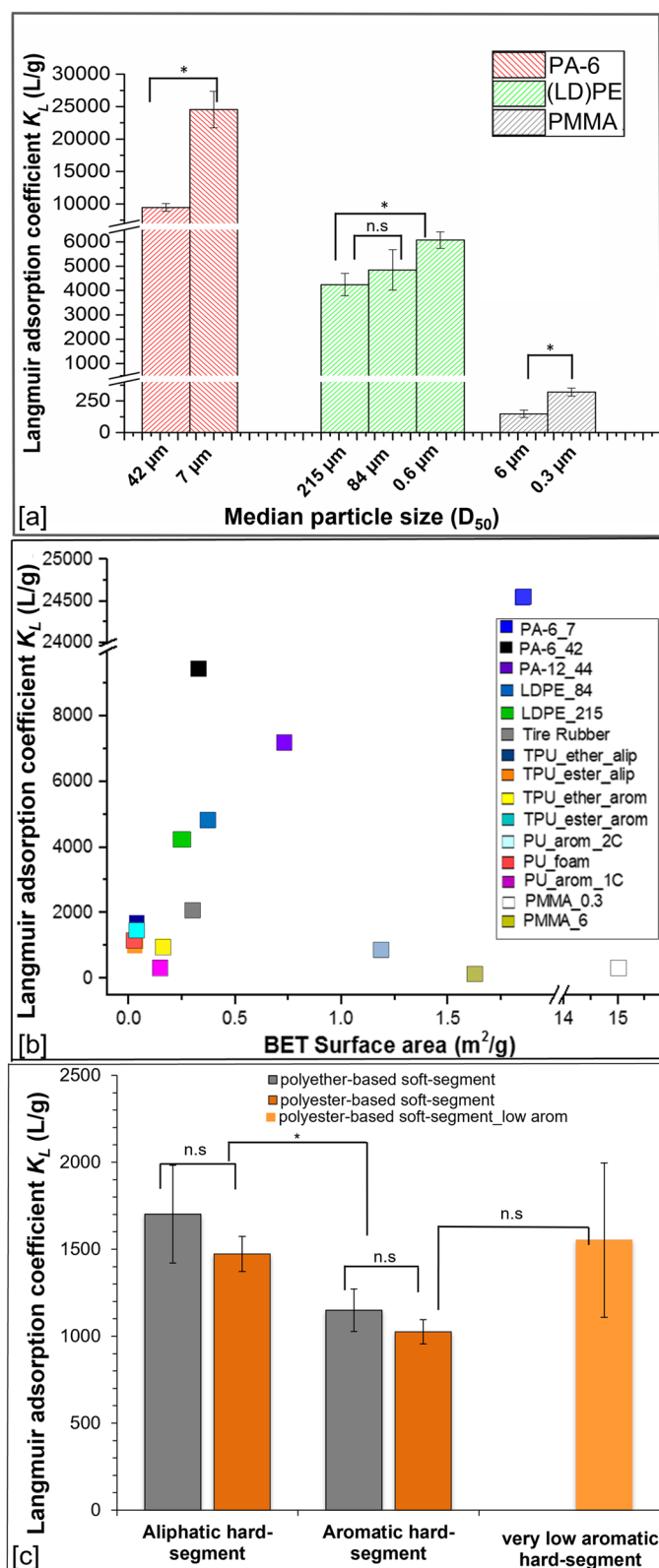
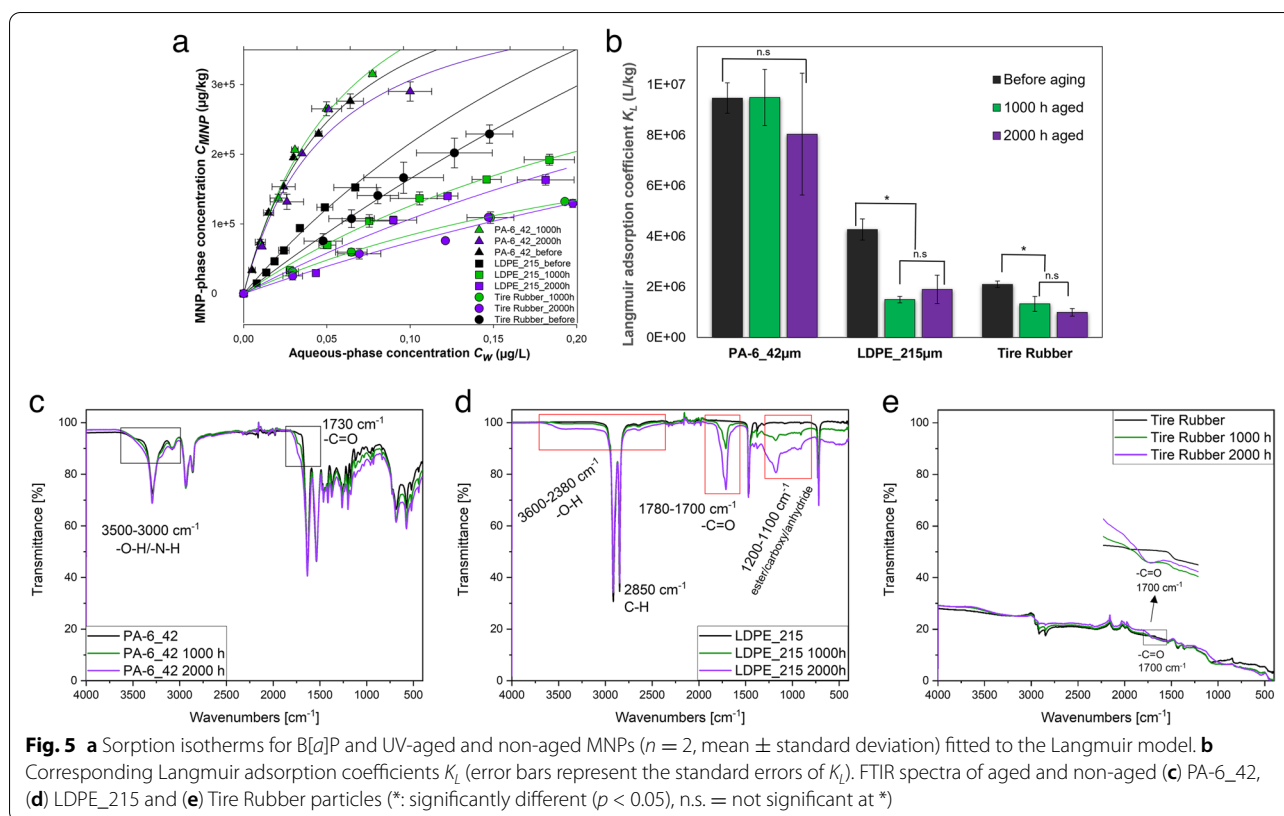


Fig. 4 **a** Effect of particle size on the Langmuir adsorption coefficient K_L for adsorption of B[a]P to MNPs of the same polymer type. **b** Plot of the dependency of K_L on BET surface areas of MNPs. **c** Effect of TPU's hard (aliphatic and aromatic) and soft (polyester or polyether) segments on K_L . Error bars represent the standard error of K_L (*: significantly different ($p < 0.05$), n.s. = not significant at *)



of 3600–3000 and 1780–1700 cm^{-1} [80, 81] after photo-aging (Fig. 5d, e). Water will sorb more strongly to those altered interfaces and thereby diminish the sorption of B[a]P by making it energetically more difficult to displace molecules from the hydration shell and, subsequently, to partition into the bulk [82–84]. While we observed a decreased sorption of hydrophobic organic pollutants such as B[a]P after photo-aging of non-polar MNPs [68], hydrophilic pollutants may sorb more strongly [33, 85].

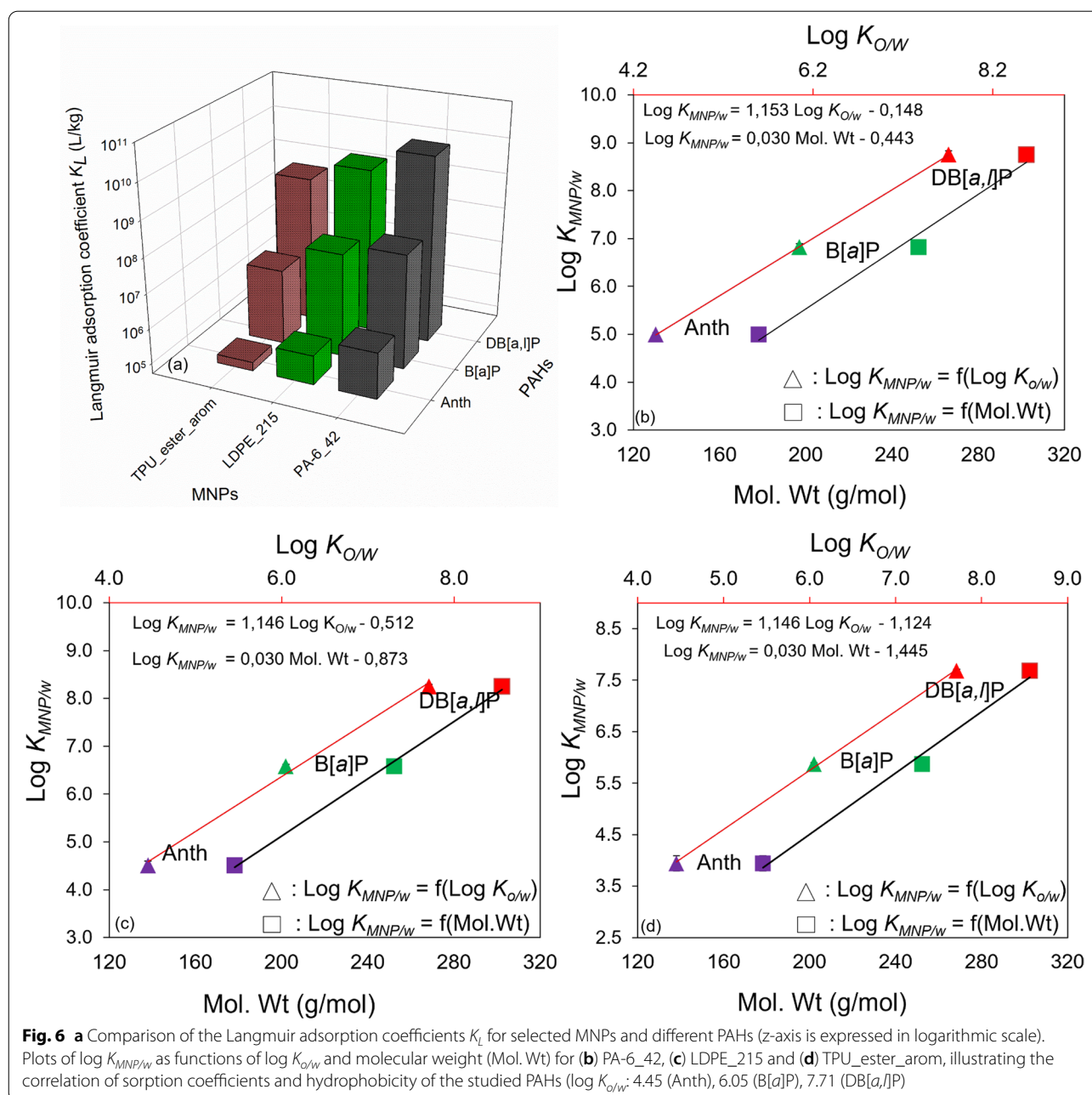
Stronger sorption to micro- and nanoplastic particles by more hydrophobic polycyclic aromatic hydrocarbons

To investigate the influence that the sorbate imposes on K_L , additional sorption isotherms of the PAHs Anth and DB[a,l]P with selected MNPs were measured. Anth, B[a]P and DB[a,l]P consist of 3, 5 and 6 condensed aromatic rings, respectively. Each sorbate/sorbent pair was studied individually in order to avoid competitive sorption, which was indeed observed in multisorbate systems and was found to be most significant for the smallest PAH Anth (see Section S6). The obtained K_L for the three investigated MNPs PA-6_42, LDPE_215 and TPU_est_aro followed the order DB[a,l]P > B[a]P > Anth (Fig. 6a) and differed by more than five orders of magnitude. For example, $\log K_L$ of sorption isotherms for TPU_est_aro increased from 3.9 (Anth) to 5.8 (B[a]P) and 7.8 (DB[a,l]

P). The same trend was observed for LDPE_215 ($\log K_L$ for Anth: 4.5, B[a]P: 6.7, DB[a,l]P: 8.4) and PA-6_42 (5.0, 7.0, 9.0). Hydrophobicity usually increases with $\log K_{o/w}$ of the sorbate [86] and may also correlate with molecular weight, in particular within a substance class [61]. Therefore, sorption coefficients $K_{MNP/w}$ (derived from the slopes of the linear parts of the isotherms, see Table S6) were plotted as a function of reported $\log K_{o/w}$ values [87, 88] and molecular weights of the PAHs (Fig. 6b–d). A linear correlation was found for both variables, suggesting that hydrophobicity of the PAHs is indeed a key factor governing their sorption to micro- and nanoplastics. This highlights the potential for a reliable prediction of the sorption coefficients of MNPs and organic pollutants within compound classes, although further experiments are required to confirm this for sorbates other than PAHs.

Conclusions

In this work we established a novel analytical TPP method that allows to reliably assess the sorption of contaminants to particulate sorbents in liquids with minimal sample preparation. The method compares favorably with the conventional batch-equilibrium approach, since it lacks laborious solvent extraction and avoids error-prone filtration and centrifugation steps. This makes the TPP method particularly suited to investigate sorption



to nano-scale particles. We demonstrated its applicability for evaluating sorption properties of a broad range of MNPs and selected PAHs at environmentally relevant concentrations. The investigated MNPs represent polymer compositions, size distributions, polydispersities and non-spherical shapes that are considered to be realistic for secondary micro- and nanoplastics originating from environmental fragmentation. We demonstrate that the key factor influencing sorption of PAHs to MNPs was the polymer type. Notably, PA-6, a polymer

used for example in AM applications, was observed to show exceptionally high sorption of B[a]P despite its relatively high polarity, which might be due to the transport of dissolved B[a]P to the bulk of the polymer. Furthermore, physico-chemical properties including particle size, polarity/hydrophobicity and polymer chain mobility were important factors modulating sorption within a given polymer type. Of note, photo-aging reduced PAH sorption, whereas more hydrophobic PAHs were sorbed more strongly.

Our data provide valuable insights toward the question whether MNPs play a significant role as carriers for POPs. Current evidence from laboratory studies, field studies and modeling suggest little relevance of MNPs as exposure sources for chemicals, mainly owing to other relevant sources of POP transfer to either marine biota [17] or humans [89]. If this is generally confirmed, our present methodology would not be needed as regulatory criterion in the context of risk assessment of plastics. However, understanding and modeling of the transport properties would still be relevant for targeting remediation activity in hot spots, where the pronounced sorption of contaminants such as PAHs to some plastics is to be considered, and exposure might be more relevant. Importantly, whereas microplastics have been discussed to potentially act as sinks for certain chemicals [90] based on their inertness and inability to enter cells, contaminated sub-micron (nanoplastic) particles may behave completely different. For example, the uptake of some nanoplastics across body barriers and into cells was recently demonstrated [91–93].

In a follow-up study we plan to investigate the *desorption* of MNP-bound pollutants in relevant media for human exposure. Understanding desorption properties constitutes the next puzzle piece towards risk assessment of MNPs, which hinges on the effective contribution of MNPs to overall POP exposure. Furthermore, we are exploring the possibility to use the sorption characteristics as a grouping criterion for MNPs.

Abbreviations

Anth: anthracene; ATR: attenuated total reflectance; B[a]P: benzo[a]pyrene; B[a]P-d₁₂: benzo[a]pyrene-d₁₂; BET: Brunauer-Emmett-Teller; CIS: cold injection system; C_{MNP}: concentration of PAHs in the MNP phase; C_{PDMS}: concentration of PAHs in the PDMS phase; C_W: concentration of PAHs in the aqueous phase; DB[a,l]P: dibenzo[a,l]pyrene; DB[a,i]P: dibenzo[a,i]pyrene; DSC: differential scanning calorimetry; FTIR: Fourier transform infrared; ISO: International Organization for Standardization; K: partition coefficient; K_L: Langmuir adsorption coefficient; K_{MNP/W}: MNP/water sorption coefficient for PAHs; K_{PDMS/W}: PDMS/water partition coefficient for PAHs; K_{o/w}: octanol/water partition coefficient; (LD)PE: (low-density) polyethylene; M_{MNP}: mass of MNPs; MNPs: micro- and nanoplastic particles; Mol. Wt: molecular weight; M_{PDMS}: mass of PDMS; m_{total}: total mass of PAH in the system; n.s.: not significant; p: probability; PA: polyamide; PA-6: polyamide 6; PAHs: polycyclic aromatic hydrocarbons; PBDEs: polybrominated diphenyl ethers; PCBs: polychlorinated biphenyls; PDMS: polydimethylsiloxane; PMMA: polymethyl methacrylate; POPs: persistent organic pollutants; PU: polyurethane; R²: coefficient of determination; SBSE: stir-bar sorptive extraction; SIM: selective ion monitoring; SLS: selective local sintering; TC: thermal conditioner; TD-GC-MS: thermal desorption gas chromatography mass spectrometry; TDU: thermal desorption unit; T_g: glass transition temperature; T_m: melting temperature; TPP: third-phase partition; TPUs: thermoplastic polyurethanes; UV: ultraviolet; V_w: volume of water; χ²: Chi-square errors.

Supplementary Information

The online version contains supplementary material available at <https://doi.org/10.1186/s43591-022-00049-9>.

Additional file 1.

Acknowledgements

This study was supported by the German Federal Institute for Risk Assessment (BfR). We thank Svetlana Kruschinski and Karsten Schön for their excellent technical assistance with TD-GC-MS measurements.

Authors' contributions

A.R. and C.H. conceptualized the study, with contributions from A.H. The experiments for this study were carried out by E.E.E., with contributions from P.M.P. (MNP aging and FT-IR spectroscopy) and D.B.B. (batch-method experiments). W.W. and P.M.P. characterized the MNPs. E.E.E. and A.R. wrote the manuscript with contributions from A.H., C.H., W.W. and P.M.P. The study was supervised by A.R. and A.H. The authors read and approved the final manuscript.

Funding

Open Access funding enabled and organized by Projekt DEAL. This work was funded by the BMBF (German Federal Ministry of Education and Research) within the InnoMat.Life project (funding no: 03XP0216X).

Availability of data and materials

Supplementary Information is available in the online version of this article.

Declarations

Ethics approval and consent to participate

Not applicable.

Consent for publication

All authors read and approved the final version of the manuscript.

Competing interests

The authors declare no competing financial interest. W.W. and P.M.P. are employees of BASF SE, a company producing and marketing polymers, including some of those investigated in this study.

Author details

¹German Federal Institute for Risk Assessment, Department of Chemical and Product Safety, Berlin, Germany. ²Bayreuth Center for Ecology and Environmental Research (BayCEER), University of Bayreuth, Bayreuth, Germany. ³BASF SE, Carl-Bosch-Str. 38, 67056 Ludwigshafen, Germany.

Received: 13 September 2022 Accepted: 5 December 2022

Published online: 26 December 2022

References

1. PlasticsEurope, Plastics – the Facts 2020: An analysis of European plastics production, demand and waste data. 2020: Brussels.
2. Environment, A.F.W. Intentionally added microplastics in products. Final report. London; 2017.
3. Alfaro-Nunez A, et al. Microplastic pollution in seawater and marine organisms across the Tropical Eastern Pacific and Galapagos. *Sci Rep*. 2021;11(1):6424.
4. Kelly A, et al. Microplastic contamination in east Antarctic sea ice. *Mar Pollut Bull*. 2020;154:111130.
5. Tamminga M, Fischer EK. Microplastics in a deep, dimictic lake of the North German Plain with special regard to vertical distribution patterns. *Environ Pollut*. 2020;267:115507.
6. Lim X. Microplastics are everywhere - but are they harmful? *Nature*. 2021;593(7857):22–5.
7. Guzzetti E, et al. Microplastic in marine organism: Environmental and toxicological effects. *Environ Toxicol Pharmacol*. 2018;64:164–71.
8. Jamieson AJ, et al. Microplastics and synthetic particles ingested by deep-sea amphipods in six of the deepest marine ecosystems on Earth. *R Soc Open Sci*. 2019;6(2):180667.
9. Zhang J, Wang L, Kannan K. Microplastics in house dust from 12 countries and associated human exposure. *Environ Int*. 2020;134:105314.
10. Barrett J, et al. Microplastic Pollution in Deep-Sea Sediments From the Great Australian Bight. *Frontiers in Marine Science*. 2020:7.

11. Senathirajah K, et al. Estimation of the mass of microplastics ingested - A pivotal first step towards human health risk assessment. *J Hazard Mater.* 2021;404(Pt B):124004.
12. Cox KD, et al. Human Consumption of Microplastics. *Environ Sci Technol.* 2019;53(12):7068–74.
13. Leslie HA, et al. Discovery and quantification of plastic particle pollution in human blood. *Environ Int.* 2022;163:107199.
14. Gigault J, et al. Nanoplastics are neither microplastics nor engineered nanoparticles. *Nat Nanotechnol.* 2021;16(5):501–7.
15. Koelmans AA, et al. Microplastics in freshwaters and drinking water: Critical review and assessment of data quality. *Water Res.* 2019;155:410–22.
16. Herzke D, et al. Negligible Impact of Ingested Microplastics on Tissue Concentrations of Persistent Organic Pollutants in Northern Fulmars off Coastal Norway. *Environ Sci Technol.* 2016;50(4):1924–33.
17. Koelmans AA, et al. Microplastic as a Vector for Chemicals in the Aquatic Environment: Critical Review and Model-Supported Reinterpretation of Empirical Studies. *Environ Sci Technol.* 2016;50(7):3315–26.
18. Gouin T. Addressing the importance of microplastic particles as vectors for long-range transport of chemical contaminants: perspective in relation to prioritizing research and regulatory actions. *Microplast Nanoplast.* 2021;1(1).
19. Kinigopoulou V, et al. Microplastics as carriers of inorganic and organic contaminants in the environment: A review of recent progress. *J Mol Liq.* 2022;350.
20. Liu L, Fokkink R, Koelmans AA. Sorption of polycyclic aromatic hydrocarbons to polystyrene nanoplastic. *Environ Toxicol Chem.* 2016;35(7):1650–5.
21. Wang W, Wang J. Different partition of polycyclic aromatic hydrocarbon on environmental particulates in freshwater: Microplastics in comparison to natural sediment. *Ecotoxicol Environ Saf.* 2018;147:648–55.
22. Teuten EL, et al. Potential for plastics to transport hydrophobic contaminants. *Environ Sci Technol.* 2007;41(22):7759–64.
23. Gao L, et al. Microplastics aged in various environmental media exhibited strong sorption to heavy metals in seawater. *Mar Pollut Bull.* 2021;169:112480.
24. Kedzierski M, et al. Threat of plastic ageing in marine environment. Adsorption/desorption of micropollutants. *Mar Pollut Bull.* 2018;127:684–94.
25. Turner A, Holmes LA. Adsorption of trace metals by microplastic pellets in fresh water. *Environ Chem.* 2015;12(5):600.
26. Cao Y, et al. A critical review on the interactions of microplastics with heavy metals: Mechanism and their combined effect on organisms and humans. *Sci Total Environ.* 2021;788:147620.
27. Zhan Z, et al. Sorption of 3,3',4,4'-tetrachlorobiphenyl by microplastics: A case study of polypropylene. *Mar Pollut Bull.* 2016;110(1):559–63.
28. Velzeboer I, Kwadijk CJ, Koelmans AA. Strong sorption of PCBs to nanoplastics, microplastics, carbon nanotubes, and fullerenes. *Environ Sci Technol.* 2014;48(9):4869–76.
29. Syberg K, et al. Sorption of PCBs to environmental plastic pollution in the North Atlantic Ocean: Importance of size and polymer type. *Case Studies in Chemical and Environmental Engineering.* 2020:2.
30. Xu P, et al. Sorption of polybrominated diphenyl ethers by microplastics. *Mar Pollut Bull.* 2019;145:260–9.
31. Wu J, et al. Effects of polymer aging on sorption of 2,2',4,4'-tetrabromodiphenyl ether by polystyrene microplastics. *Chemosphere.* 2020;253:126706.
32. Wang W, Wang J. Comparative evaluation of sorption kinetics and isotherms of pyrene onto microplastics. *Chemosphere.* 2018;193:567–73.
33. Liu G, et al. Sorption behavior and mechanism of hydrophilic organic chemicals to virgin and aged microplastics in freshwater and seawater. *Environ Pollut.* 2019;246:26–33.
34. Lee H, Shim WJ, Kwon JH. Sorption capacity of plastic debris for hydrophobic organic chemicals. *Sci Total Environ.* 2014;470:1545–52.
35. Bakir A, Rowland SJ, Thompson RC. Transport of persistent organic pollutants by microplastics in estuarine conditions. *Estuar Coast Shelf Sci.* 2014;140:14–21.
36. Shahrubudin N, Lee TC, Ramlan R. An Overview on 3D Printing Technology: Technological, Materials, and Applications. *Proc Manuf.* 2019;35:1286–96.
37. Fan D, et al. Progressive 3D Printing Technology and Its Application in Medical Materials. *Front Pharmacol.* 2020;11:122.
38. Sigloch H, et al. 3D Printing - Evaluating Particle Emissions of a 3D Printing Pen. *J Vis Exp.* 2020;164.
39. (EU), C.R., 1245 of 2 September 2020 amending and correcting Regulation (EU) No 10/2011 on plastic materials and articles intended to come into contact with food in OJ L 288. 2020. p. 1–17.
40. Koelmans AA, et al. Risk assessment of microplastic particles. *Nat Rev Mat.* 2022;7(2):138–52.
41. Mu Q, et al. Temperature effect on phase state and reactivity controls atmospheric multiphase chemistry and transport of PAHs. *Sci Adv.* 2018;4(3):eaap7314.
42. Agrawal S, Kaur AP, Taneja K. A Comprehensive Review of Benzo Alpha Pyrene (B[*A*]P) Toxicology. *Res J Pharm Biol Chem Sci.* 2018;9(4):1049–58.
43. Verma N, et al. Review on proteomic analyses of benzo[*a*]pyrene toxicity. *Proteomics.* 2012;12(11):1731–55.
44. EEC, COUNCIL DIRECTIVE 67/548/EEC of 27 June 1967 on the approximation of laws, regulations and administrative provisions relating to the classification, packaging and labelling of dangerous substances. 1967. p. 1–357.
45. ECHA, Guidance on information requirements and chemical safety assessment, Chapter R.8: Characterisation of dose [concentration]-response for human health. 2008. p. 1–150.
46. EC, Regulation (EC) No. 1272/2008 of the European Parliament and of the Council of 16 December 2008 on classification, labelling and packaging of substances and mixtures, amending and repealing Directives 67/548/EEC and 1999/45/EC, and amending Regulation. *Official Journal of the European Union*, 2008(L 353-1-L 353/1355): p. .
47. Delistraty D. Toxic equivalency factor approach for risk assessment of polycyclic aromatic hydrocarbons. *Toxicol Environ Chem.* 1997;64(1-4):81–108.
48. Li J, Zhang K, Zhang H. Adsorption of antibiotics on microplastics. *Environ Pollut.* 2018;237:460–7.
49. Rochman CM, et al. Long-term field measurement of sorption of organic contaminants to five types of plastic pellets: implications for plastic marine debris. *Environ Sci Technol.* 2013;47(3):1646–54.
50. Gocht T, Klemm O, Grathwohl P. Long-term atmospheric bulk deposition of polycyclic aromatic hydrocarbons (PAHs) in rural areas of Southern Germany. *Atmos Environ.* 2007;41(6):1315–27.
51. Romagnoli P, et al. Indoor PAHs at schools, homes and offices in Rome, Italy. *Atmos Environ.* 2014;92:51–9.
52. Jonker MTO, Koelmans AA. Polyoxymethylene solid phase extraction as a partitioning method for hydrophobic organic chemicals in sediment and soot. *Environ Sci Technol.* 2001;35(18):3742–8.
53. OECD Guideline for the testing of chemicals: Adsorption - Desorption Using a Batch Equilibrium Method. 2000.
54. ISO, D.E., Plastics - Methods of exposure to laboratory light sources - Part 2: Xenon-arc lamps (ISO 4892-2:2013). 2013. p. 20.
55. Pfohl P, et al. Microplastic extraction protocols can impact the polymer structure. *Microplast Nanoplast.* 2021;1(1):1.
56. Kah M, et al. Measuring and modeling adsorption of PAHs to carbon nanotubes over a six order of magnitude wide concentration range. *Environ Sci Technol.* 2011;45(14):6011–7.
57. Cornelissen G, vanNoort PCM, Govers HAJ. Desorption kinetics of chlorobenzenes, polycyclic aromatic hydrocarbons, and polychlorinated biphenyls: Sediment extraction with Tenax(R) and effects of contact time and solute hydrophobicity. *Environ Toxicol Chem.* 1997;16(7):1351–7.
58. ISO/IEC, Uncertainty of measurement — Part 3: Guide to the expression of uncertainty in measurement (GUM:1995). 2008. p. 120.
59. Harter RD, Baker DE. Applications and Misapplications of the Langmuir Equation to Soil Adsorption Phenomena. *Soil Sci Soc Am J.* 1977;41(6):1077–80.
60. DiFilippo EL, Eganhouse RP. Assessment of PDMS-water partition coefficients: implications for passive environmental sampling of hydrophobic organic compounds. *Environ Sci Technol.* 2010;44(18):6917–25.
61. Grant S, et al. Experimental Solubility Approach to Determine PDMS-Water Partition Constants and PDMS Activity Coefficients. *Environ Sci Technol.* 2016;50(6):3047–54.
62. Ayawei N, Ebelegi AN, Wankasi D. Modelling and Interpretation of Adsorption Isotherms. *J Chem.* 2017;2017:1–11.
63. Gupta S, Kumar A. Removal of nickel (II) from aqueous solution by biosorption on A. barbadensis Miller waste leaves powder. *Applied Water Science.* 2019;9(4):1.

64. Fu L, et al. Adsorption behavior of organic pollutants on microplastics. *Ecotoxicol Environ Saf*. 2021;217:112207.
65. Belhachemi M, Addoun F. Comparative adsorption isotherms and modeling of methylene blue onto activated carbons. *App Water Sci*. 2011;1(3-4):111–7.
66. www.ultramid.de, Ultramid® (PA): Product Brochure, BASF, 2013.
67. Extrand CW. Water contact angles and hysteresis of polyamide surfaces. *J Colloid Interface Sci*. 2002;248(1):136–42.
68. Huffer T, Hofmann T. Sorption of non-polar organic compounds by micro-sized plastic particles in aqueous solution. *Environ Pollut*. 2016;214:194–201.
69. Wright SL, Thompson RC, Galloway TS. The physical impacts of microplastics on marine organisms: a review. *Environ Pollut*. 2013;178:483–92.
70. Agboola OD, Benson NU. Physisorption and Chemisorption Mechanisms Influencing Micro (Nano) Plastics-Organic Chemical Contaminants Interactions: A Review. *Front Environ Sci*. 2021;9.
71. Pascall MA, et al. Uptake of polychlorinated biphenyls (PCBs) from an aqueous medium by polyethylene, polyvinyl chloride, and polystyrene films. *J Agric Food Chem*. 2005;53(1):164–9.
72. Gilbert D, et al. Polymers as Reference Partitioning Phase: Polymer Calibration for an Analytically Operational Approach To Quantify Multimedia Phase Partitioning. *Anal Chem*. 2016;88(11):5818–26.
73. Lohmann R. Critical review of low-density polyethylene's partitioning and diffusion coefficients for trace organic contaminants and implications for its use as a passive sampler. *Environ Sci Technol*. 2012;46(2):606–18.
74. Guo X, et al. Sorption of four hydrophobic organic compounds by three chemically distinct polymers: role of chemical and physical composition. *Environ Sci Technol*. 2012;46(13):7252–9.
75. Liu X, et al. Microplastics as Both a Sink and a Source of Bisphenol A in the Marine Environment. *Environ Sci Technol*. 2019;53(17):10188–96.
76. Mohamed Nor NH, Koelmans AA. Transfer of PCBs from Microplastics under Simulated Gut Fluid Conditions Is Biphasic and Reversible. *Environ Sci Technol*. 2019;53(4):1874–83.
77. Holmes LA, Turner A, Thompson RC. Adsorption of trace metals to plastic resin pellets in the marine environment. *Environ Pollut*. 2012;160(1):42–8.
78. Wang J, et al. Size effect of polystyrene microplastics on sorption of phenanthrene and nitrobenzene. *Ecotoxicol Environ Saf*. 2019;173:331–8.
79. Berens AR. Analysis of transport behavior in polymer powders. *J Membr Sci*. 1978;3(2):247–64.
80. Beachell HC, Chang IL. Photodegradation of urethane model systems. *Journal of Polymer Science Part A-1. Polymer Chem*. 1972;10(2):503–20.
81. Roger A, Sallet D, Lemaire J. Photochemistry of aliphatic polyamides. 4. Mechanisms of photooxidation of polyamides 6, 11, and 12 at long wavelengths. *Macromolecules*. 2002;19(3):579–84.
82. Pan B, Xing B. Adsorption mechanisms of organic chemicals on carbon nanotubes. *Environ Sci Technol*. 2008;42(24):9005–13.
83. Ania CO, et al. Effects of activated carbon properties on the adsorption of naphthalene from aqueous solutions. *Appl Surf Sci*. 2007;253(13):5741–6.
84. Huffer T, Weniger AK, Hofmann T. Sorption of organic compounds by aged polystyrene microplastic particles. *Environ Pollut*. 2018;236:218–25.
85. Holmes LA, Turner A, Thompson RC. Interactions between trace metals and plastic production pellets under estuarine conditions. *Mar Chem*. 2014;167:25–32.
86. Zhao L, et al. Sorption of five organic compounds by polar and nonpolar microplastics. *Chemosphere*. 2020;257:127206.
87. National center for biotechnology information, PubChem Compound Summary for CID 9119, Dibenzo[a,h]pyrene. 2022.
88. Hansch, C.L., Leo A; Hoekman, D, Exploring QSAR: Hydrophobic, Electronic, and Steric Constants C.L. Hansch, A; Hoekman, DH Editor. 1995 American Chemical Society.
89. Mohamed Nor NH, et al. Lifetime Accumulation of Microplastic in Children and Adults. *Environ Sci Technol*. 2021;55(8):5084–96.
90. Gouin T, et al. A thermodynamic approach for assessing the environmental exposure of chemicals absorbed to microplastic. *Environ Sci Technol*. 2011;45(4):1466–72.
91. Domenech J, et al. Interactions of polystyrene nanoplastics with in vitro models of the human intestinal barrier. *Arch Toxicol*. 2020;94(9):2997–3012.
92. Lehner R, et al. Emergence of Nanoplastic in the Environment and Possible Impact on Human Health. *Environ Sci Technol*. 2019;53(4):1748–65.
93. Paul MB, et al. Beyond microplastics - investigation on health impacts of submicron and nanoplastic particles after oral uptake in vitro. *Microplast Nanoplast*. 2022;2(1).

Publisher's Note

Springer Nature remains neutral with regard to jurisdictional claims in published maps and institutional affiliations.

Submit your manuscript to a SpringerOpen[®] journal and benefit from:

- Convenient online submission
- Rigorous peer review
- Open access: articles freely available online
- High visibility within the field
- Retaining the copyright to your article

Submit your next manuscript at ► [springeropen.com](https://www.springeropen.com)